Naval Research Laboratory
Washington, DC 20375-5320

NRL/6880/MR—2024/2

Production of Diverse Functional Core/Shell Nanoparticles via Atomic Layer Deposition

BENJAMIN GREENBERG

Power and Advanced Materials Branch
Electronics Science and Technology Division

May 5, 2024

REPORT DOCUMENTATION PAGE

PLEASE DO NOT RETURN YOUR FORM TO THE ABOVE ORGANIZATION

1. REPORT DATE	2. REPORT TYPE	3. DATES COVERED	
05-05-2024	NRL Memorandum Report	START DATE 04/26/2021	END DATE 04/25/2022

4. TITLE AND SUBTITLE
Production of Diverse Functional Core/Shell Nanoparticles via Atomic Layer Deposition

5a. CONTRACT NUMBER	5b. GRANT NUMBER	5c. PROGRAM ELEMENT NUMBER
		NISE
5d. PROJECT NUMBER	**5e. TASK NUMBER**	**5f. WORK UNIT NUMBER**
		N20F

6. AUTHOR(S)
Benjamin Greenberg

7. PERFORMING ORGANIZATION / AFFILIATION NAME(S) AND ADDRESS(ES)
Naval Research Laboratory
4555 Overlook Ave SW
Washington, DC 20375-5320

8. PERFORMING ORGANIZATION REPORT NUMBER
NRL/6880/MR—2024/2

9. SPONSORING / MONITORING AGENCY NAME(S) AND ADDRESS(ES)	10. SPONSOR / MONITOR'S ACRONYM(S) NUMBER	11. SPONSOR / MONITOR'S REPORT NUMBER(S)
Naval Research Laboratory 4555 Overlook Ave SW Washington, DC 20375-5320	NRL	

12. DISTRIBUTION / AVAILABILITY STATEMENT
DISTRIBUTION STATEMENT A: Approved for public release; distribution is unlimited.

13. SUPPLEMENTAL NOTES
Karles Fellowship

14. ABSTRACT
In this work, we develop rotary particle ALD (pALD) processes for depositing Au on TiN and TiO2 nanoparticles (NPs) for optical applications, and we investigate ZnO ALD infilling of macroscopic porous compacts of Al2O3 NPs. Au pALD produces Au NPs that decorate the surfaces of the TiN and TiO2 particles. We also use rotary pALD to deposit ZnO shells on Al2O3 NPs, and we compare a ZnO-infilled Al2O3 NP compact to a compact formed by pressing pALD-produced core/shell Al2O3/ZnO NPs in order to elucidate the effects of the very long ALD precursor dose times necessary for complete infilling of macroscopic nanoporous solids.

15. SUBJECT TERMS
Atomic layer deposition, nanoparticles

16. SECURITY CLASSIFICATION OF:			17. LIMITATION OF ABSTRACT	18. NUMBER OF PAGES
a. REPORT	b. ABSTRACT	c. THIS PAGE	SAR	13
U	U	U		

19a. NAME OF RESPONSIBLE PERSON	19b. PHONE NUMBER *(Include area code)*
Benjamin Greenberg	(202) 404-3862

This page intentionally left blank.

CONTENTS

This page intentionally left blank.

PRODUCTION OF DIVERSE FUNCTIONAL CORE/SHELL NANOPARTICLES VIA ATOMIC LAYER DEPOSITION

1. INTRODUCTION

1.1 Core/shell nanoparticles via particle atomic layer deposition (pALD)

Core/shell nanoparticles (NPs)—spheroids with diameter on the order of 100 nm or less enveloped in shells of a material distinct from the spheroid material—have unique properties due to their small size and the combination of two different materials on the nanoscale. Applications include optical, electronic, structural, refractory, and smart materials. A variety of core/shell NPs have been produced by liquid- and gas-phase techniques; for example, semiconductor heterojunction core/shell NPs have been produced by colloidal synthesis [1] and nonthermal plasma synthesis [2]. The materials accessible by these techniques, however, are limited by a number of factors such as the solvent boiling point in the case of colloidal synthesis (which limits synthesis temperature) and heterogeneous nucleation in the case of plasma synthesis (the formation of separate particles of shell material, which makes shells of compound materials particularly difficult to produce).

Particle atomic layer deposition (pALD) has emerged in the last two decades as a versatile route to scalable production of a wide variety of core/shell NPs, including many that are difficult to synthesize by other methods [3]. In the pALD approach, the core NPs can be produced by any method, including "top-down" methods such as ball milling and laser ablation as well as "bottom-up" techniques such as colloidal and plasma synthesis. The shells are then deposited on a powder of the core NPs using a pALD reactor, which is an atomic layer deposition (ALD) reactor specifically designed for deposition on particle powders. In general, ALD produces conformal coatings with atomic scale thickness control via alternating exposures of at least two different precursor gases or vapors, each of which deposits approximately one atomic layer per exposure via a self-limiting reaction. In conventional ALD, the prototypical substrate is a semiconductor wafer. In pALD, to enable conformal coating of individual particles, the powder substrates is continuously agitated via either gas flow (in the case of a fluidized bed reactor, FBR) or rotary motion [4].

In this work, we develop rotary pALD processes for depositing Au on TiN and TiO_2 particles for optical applications and ZnO on Al_2O_3 particles for a fundamental study of ALD reaction-diffusion. In the case of Au pALD, the coating takes the form of Au NPs that decorate the surfaces of the TiN and TiO_2 particles. Our Au pALD results are summarized in sections 3.1 and 3.2; versions of these sections were included in the Memorandum Report, "Visible-Light Activated Sensor for Detection of Chemical Warfare Agent Simulants" by Baturina et al. [5]. In the cases of Al_2O_3 and ZnO pALD, the coatings are continuous shells that completely envelope particles and/or agglomerates of particles. For some applications, the core/shell powders can be sintered via environmentally controlled pressure-assisted sintering (EC-PAS), an NRL-developed process that transforms NP powders into fully dense nanocomposite solids.

1.2 Atomic layer deposition (ALD) infilling of porous nanoparticle (NP) compacts

In an ideal nanocomposite solid produced by EC-PAS of a core/shell NP powder, the NP cores are isolated and only the shell material percolates; i.e., only the shell material forms continuous networks that traverse the entire solid. This morphology is useful for many applications, but some applications require continuous networks of the core material. Therefore, in addition to developing pALD processes, we develop an alternative ALD technique for producing nanocomposites: ALD infilling of porous NP compacts. Uncoated NPs are pressed to form porous compacts, and then ALD is used to coat conformally the internal surfaces of the compacts without disrupting the continuous networks of NPs. At the same time, the coating itself forms a continuous network. The ALD-infilled compact can then be sintered by EC-PAS to form a nanocomposite solid in which both materials percolate.

Manuscript approved April 15, 2024.

In this work, we develop a process for infilling Al_2O_3 NP compacts with ZnO for a fundamental study of ALD reaction-diffusion. Specifically, we compare the ZnO-infilled Al_2O_3 NP compact to a compact formed by pressing pALD-produced core/shell Al_2O_3/ZnO NPs in order to elucidate the effects of the very long ALD precursor dose times necessary for complete infilling of macroscopic nanoporous solids.

2. METHODS

Atomic layer deposition (ALD) infilling and particle atomic layer deposition (pALD) of Au, Al_2O_3, and ZnO were performed using a Forge Nano (formerly ALD NanoSolutions) RX-series rotary reactor equipped with a titanium alloy rotary drum. The precursors for these processes were trimethyl(trimethylphosphine)gold (Me_3AuPMe_3), O_3, and H_2O; trimethylaluminum (TMA) and H_2O; and diethylzinc (DEZ) and H_2O; respectively. The Me_3AuPMe_3 cylinder was heated to 85 °C, while the TMA, DEZ, and H_2O cylinders remained at room temperature. O_3 was supplied by an IN USA (Teledyne API) AC-2000 ozone generator operated at 70% power and an O_2 flow rate of 120 SCCM.

Transmission electron micrographs of the NPs were obtained using a JEOL 2200FS transmission electron microscope (TEM) operated at an accelerating voltage of 200 kV. TEM specimens were prepared by dispersing NPs in ethanol, ultrasonicating the dispersion, and dropcasting the dispersion onto a copper grid with a continuous carbon support film. The specific surface areas of the NP powders were determined via the Brunauer−Emmett−Teller (BET) method using a Micromeritics ASAP 2020 surface area and porosimetry system. The sample tube was filled with powder and sealed inside an N_2 glovebox, and prior to measurement, the coated powders were degassed at a nominal temperature of 450 °C. X-ray diffraction (XRD) patterns were obtained using a Rigaku X-ray powder diffractometer equipped with a Cu Kα 18 kW rotating anode source. UV-vis spectra were acquired using a Perkin-Elmer UV/VIS/NIR λ 1050 spectrometer equipped with an integrated sphere. Scanning electron microscopy (SEM) was performed with a ThermoFisher Scientific Quattro environmental scanning electron microscope operated at an accelerating voltage ranging from 10 to 20 kV. Ellipsometry spectra were acquired using a J.A. Woollam Alpha-SE ellipsometer.

3. RESULTS AND DISCUSSION

3.1 pALD of Au on TiN NPs

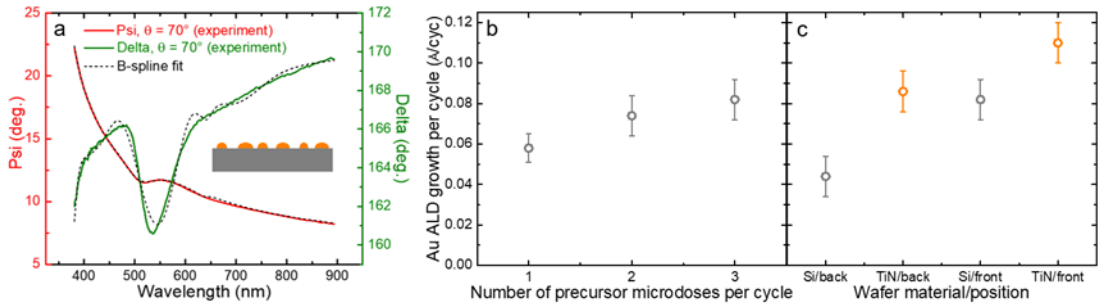

Fig. 1 — (a) Representative ellipsometry spectra for Au islands deposited on a Si wafer. (b) Au ALD growth per cycle as a function of the number of Me3AuPMe3 microdoses per cycle. (c) Au ALD growth per cycle for various substrate materials and positions within the pALD drum.

To prepare for Au pALD on TiN nanopowder, we first developed an ALD recipe for depositing Au on Si and TiN wafers, building upon the Au ALD work of Griffiths et al. [6]. An Au ALD cycle consists of

Me_3AuPMe_3, O_3, and H_2O doses, and each doses can consist of multiple microdoses. Holding the number of cycles at 50 and deposition temperature at 105 °C and positioning a Si wafer in the front of the rotary drum—which contains the TiN powder in pALD experiments—we varied the number of microdoses from 1 to 3 and measured the quantity of Au deposited by ellipsometry (Fig. 1). The spectral line shape of psi, peaked rather than sigmoidal, indicated that we deposited Au islands rather than a continuous thin film, which is generally expected for a 50 cycle deposition. Using a B-spline fitting of psi and delta to quantify the deposited Au in terms an effective film thickness, we found that 3 microdoses produced a reasonable growth per cycle (GPC) of ~0.08 A/cyc on the Si wafer. We then used this recipe to deposit 50 cycles of Au on Si and TiN wafers placed in the front and back of the drum. GPC in the back of the drum is particularly important, because this is where TiN powder is located for pALD. We found that while GPC on Si wafers is 50% lower in the back of the drum, this effect is cancelled out by the generally higher GPC on TiN wafers, so that the GPC on a TiN wafer in the back of the drum is still ~0.08 A/cyc (Fig. 1).

Based on the encouraging results of these Au ALD experiments, we proceeded to develop a particle ALD (pALD) recipe for coating TiN NPs with Au. To deposit Au on a substrate with a much larger surface area, we increased the number of microdoses from 3 to 4, and we increased the microdose hold times (the time that the precursor is held in the chamber after the pulse to allow the reaction to continue): from 8 to 30 s for Me_3AuPMe_3, from 0 to 30 s so for O_3, and from 16 to 60 s for H_2O. For O_3 and H_2O, we also increased the pulse times (from 16 to 40 s and from 2 to 3 s, respectively), whereas for Me_3AuPMe_3, we did not increase the pulse time, because no additional vapor could be obtained from a longer pulse—i.e., Me_3AuPMe_3 delivery is evaporation-rate-limited. The Au deposition temperature was 105 or 110 °C depending on the location of the substrate.

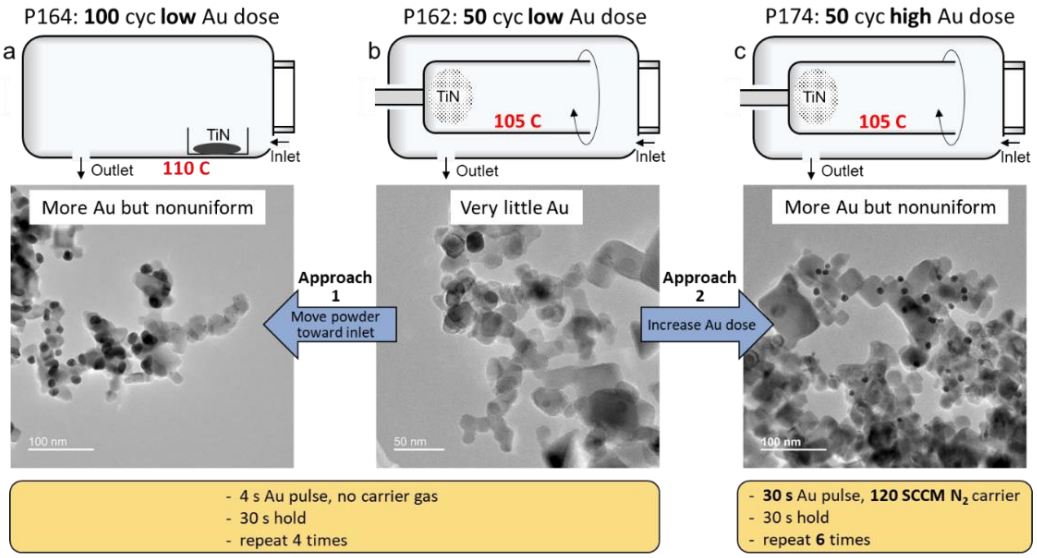

Fig. 2 — Schematics of Au pALD trials and TEM of resultant Au-coated TiN NPs: (a) P164, (b) P162, (c) P174

Fig. 2 shows the results of three Au pALD trials numbered P162, P164, and P174. In P162, 20 mg of TiN NP powder was placed in the typical position in the back of the rotary drum, and the drum was rotated to agitate the powder. As shown in Fig. 2b, this procedure resulted in very little Au deposition on the TiN powder. In principle, the amount of Me_3AuPMe_3 delivered to the powder can be increased by two approaches: moving the powder closer to the pALD reactor inlet (Approach 1) and increasing the overall quantity of Me_3AuPMe_3 in the chamber (Approach 2). For P164, we used Approach 1, positioning the powder in a boat directly in front of the chamber inlet in order to maximize Me_3AuPMe_3 exposure (which

unfortunately meant that agitation was not possible, because the powder was not inside the rotary drum), and we increased the number of Au ALD cycles to 100. This run resulted in significantly more Au deposition in some regions of the TiN powder, but the deposition was nonuniform (some regions contained no Au). For P174, we used Approach 2, increasing the number of Me_3AuPMe_3 microdoses per cycle from 4 to 6 and the Au pulse time in each microdose from 4 s to 30 s. Also, during each pulse a 120 SCCM N_2 flow was added over the open Me_3AuPMe_3 cylinder to boost the Me_3AuPMe_3 evaporation rate and enable delivery of a greater quantity in each pulse. TEM reveals that Approach 2 significantly increased the quantity of Au deposited on the TiN powder; however, the deposition was nonuniform, and large regions of the TiN powder remain virtually uncoated (Fig. 2c). These results are very similar to the results of Approach 1 (Fig. 2a); note that 100 Au pALD cycles were used to test Approach 1 vs. 50 cycles used to test Approach 2. Given that the powder is agitated in Approach 2, the nonuniformity is likely due not to uneven exposure of nanoparticle surfaces to the precursor but rather to the overall precursor quantity still being insufficient, despite the large improvement achieved by modifying the dosing procedure. Overall our results suggest that reasonably high Au deposition rates are obtainable via further development of the precursor dosing procedure.

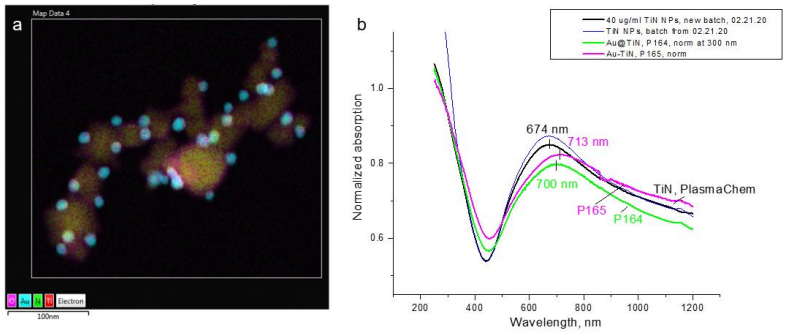

Fig. 3 — (a) STEM/EDS elemental mapping of P164: 100 cycles Au pALD on TiN NPs. (b) UV-vis spectra of P164 and P165: 200 cycles Au pALD on TiN NPs with spectra of uncoated TiN NPs for comparison.

As shown in Fig. 3, further characterization of samples produces by Approach 1 (P164 and P165, which was the same as P164 but with 200 Au pALD cycles instead of 100 Au pALD cycles) confirmed that these samples do not have the targeted morphology and optical properties. STEM/EDS elemental mapping of the P164 sample (Fig. 3a) showed Au particles without any signs of coalescence or thin Au shell formation. UV-vis spectra of aqueous suspensions of the two samples (Fig. 3b) revealed slightly redshifted absorption without enhancement, which is consistent with the formation of Au particles.

3.2 pALD of Au on TiO_2 NPs with and without Al_2O_3 pALD prior to Au pALD

For this study, we used commercial P25 TiO_2 nanopowder and we investigated the effect on Au deposition of pre-coating the TiO_2 with Al_2O_3 via pALD. We hypothesized that the Al_2O_3 coating could enhance Au deposition by increasing the surface energy of the nanopowder. As shown in Fig. 4, in each experiment, we deposited 5 cycles of Al_2O_3 on P25 TiO_2 powder (as well as a Si wafer witness) at 70, 110, or 150 and then deposited 50 cycles of Au at 110 °C. Fig. 4b shows the UV-vis spectra of the resultant TiO_2/Al_2O_3/Au powders as well as the spectra of TiO_2/Au (50 cycles of Au with no Al_2O_3) and uncoated TiO_2 samples. The plasmonic absorption near 550 nm is enhanced by the Al_2O_3 nucleation layer deposited at 150 °C and further enhanced by Al_2O_3 deposited at 110 °C; it is not enhanced, however, by Al_2O_3 deposited at 70 °C (the reason for the low baseline absorption of this sample is not clear at this time; regardless, the lack of enhanced plasmonic absorption is clear). The greater efficacy of 110 °C Al_2O_3 relative to 150 °C Al_2O_3 is consistent with our previous preliminary results, and the inefficacy of 70 °C

Al_2O_3 indicates that Au deposition is maximized at some intermediate Al_2O_3 deposition temperature (likely not far from 110 C). Perhaps, as Al_2O_3 deposition temperature is lowered, there is a tradeoff between increasing the Al_2O_3 surface energy (which promotes Au nucleation and growth) and decreasing the comformality and completeness of the Al_2O_3 coating (which leaves uncoated TiO_2 that is less conducive to Au nucleation and growth).

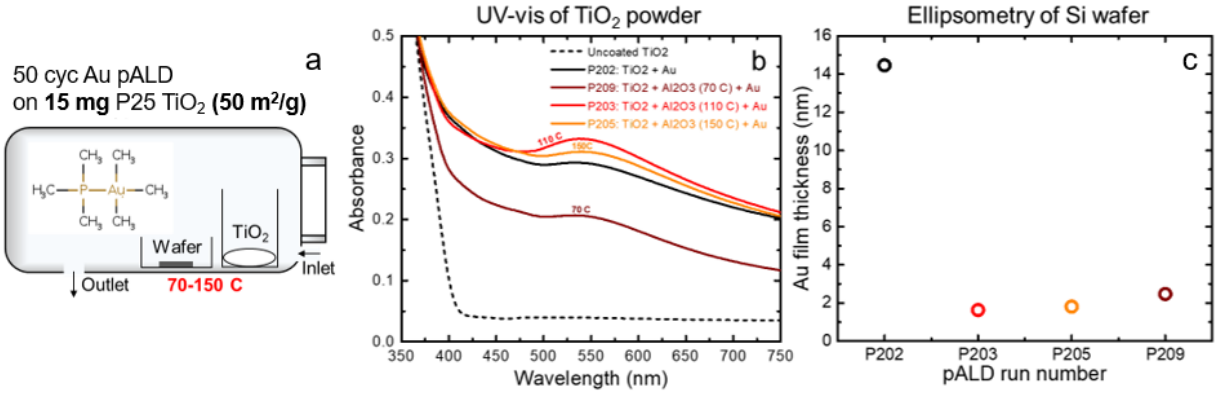

Fig. 4 — Au pALD on P25 TiO_2 NP powder without and with Al_2O_3 pALD at varied temperature prior to Au pALD: P202, P203, P205, P209. (a) Schematic of reactor configuration. (b) UV-vis spectra. (c) Equivalent film thickness, from ellipsometry, of Au coatings on witness Si wafers.

As for the Au deposited on the Si witness wafers, the equivalent film thickness measured via ellipsometry (Fig. 4c) was between 1.5 and 2.5 nm for the three Al_2O_3/Au experiments (a typical range for 50 cycles Au pALD) but, strikingly, was nearly 15 nm in the case of Au pALD without Al_2O_3 pALD. We note that this Au-pALD-only run (P202) was the first in the series and was preceded by removal, cold storage, and reattachment of the Au precursor (Me_3AuPMe_3), and in the future we will monitor for any signs that this procedure temporarily increases the Au pALD growth per cycle. A possibility to consider is that the Me_3AuPMe_3 has partially decomposed over time and is no longer a homogeneous liquid. In the meantime, the apparent lack of proportionally enhanced Au deposition on the TiO_2 powder in run P202 suggests that we are operating in a pALD regime in which the general amenability of the powder surface to Au nucleation and growth is more important than the quantity of Me_3AuPMe_3 delivered to the chamber.

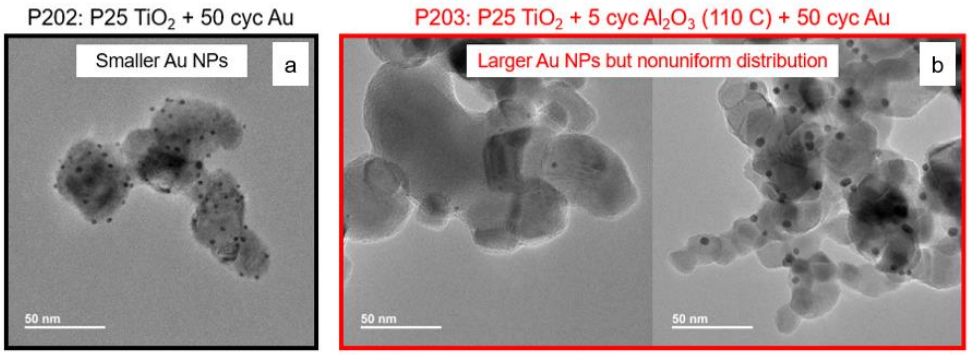

Fig. 5 — TEM of Au-coated P25 TiO_2 NP powder. (a) P202: without Al_2O_3 pALD prior to Au pALD. (b) P203: with Al_2O_3 pALD prior to Au pALD.

We used TEM to obtain a better understanding of the differences between the P202 and P203 Au-coated TiO_2 nanopowders. Fig. 5a shows that the P202 TiO_2/Au nanopowders contains relatively small Au nanoparticles (NPs), while Fig. 5b shows that the P203 TiO_2/Al_2O_3/Au nanopowder contains relatively large Au NPs; however, the Au NPs are not distributed uniformly throughout the sample, and some regions contain very few Au NPs.

3.3 ALD infilling of Al_2O_3 porous compacts with Al_2O_3

Previously, ALD has been used to infill nanoporous solids with thickness generally on the order of a few μm or smaller. For example, Cendejas et al. [7] infilled GaN NP films with ~16 nm NP diameter and film thickness <2 μm with ZnO via ALD. To predict the DEZ and H_2O dose and purge times necessary for a uniform infill, they built upon a reaction-diffusion model developed by Yanguas-Gil and Elam [8]. The model of Cendejas et al. predicted that DEZ and H_2O pulse times on the order of ~1 s would be sufficient for infilling the GaN NP films, and their experiments validated this prediction. In the present work, Al_2O_3 ALD is used to infill nanoporous solids that are ~1,000 times thicker: nanoporous compacts of Al_2O_3 NPs with ~100 nm NP diameter (15 m^2/g BET surface area) and ~2 mm compact thickness. Fig. 6 shows a schematic (Fig. 6a) and cross-sectional SEM (Fig. 6b) of an Al_2O_3 compact as well as a prediction of the required TMA dose time based on the model of Cendejas et al. The compact is mounted on a curved quartz boat so that ALD precursors can diffuse into the bottom of the compact as well as the top, reducing the required precursor diffusion length to ~1 mm. As shown in Fig. 6c, for an ALD temperature of 170 °C, TMA partial pressure of 6 Torr, and compact void volume fraction of ϕ = 49%, the predicted necessary TMA dose time is ~20 min.

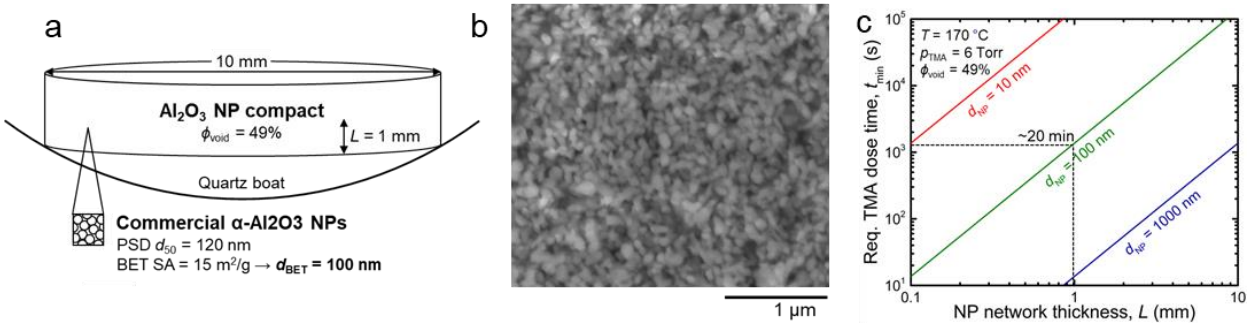

Fig. 6 — (a) Schematic of Al2O3 porous compact. (b) SEM of Al2O3 porous compact cross-section before ALD. (c) Predicted required TMA dose time as a function of NP network thickness for NP sizes: 10, 100, and 1,000 nm.

Two Al_2O_3 compacts were simultaneously infilled with ALD using a TMA partial pressure of ~6 Torr, an H_2O partial pressure of ~9 Torr, and hold and purge times of 25 and 21 min, respectively, for both precursors. The deposition temperature was ~150 °C, and the number of Al_2O_3 ALD cycles was 40, so that the total ALD process time was ~60 hr. Fig. 7 shows photographs of a compact before (Fig. 7a) and after (Fig. 7b) Al_2O_3 ALD. As expected for Al_2O_3 deposition on and Al_2O_3 substrate, there is no significant color change. There is, however, a 32% mass gain for both porous compacts, which if we assume a uniform infill of the porous compact, translates to a reduction in the porosity from ϕ = 49% to ϕ = 32%. This can be converted to an Al_2O_3 conformal coating thickness estimate by assuming either spherical NPs or spherical pores; an average of these two estimates yields a coat thinckness of 5.6 nm, or an ALD growth per cycle (GPC) of 1.4 Å/cyc, which is indeed a reasonable GPC for Al_2O_3 ALD on a nanostructured substrate [9].

Fig. 8 shows ALD chamber pressure traces during TMA doses. During the TMA pulse (the first 5 s of the dose), the pressure rises sharply as TMA fills the chamber. Subsequently, during the 25 min TMA hold

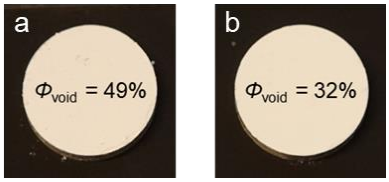

Fig. 7 — Photographs of Al2O3 porous compacts (a) before ALD and (b) after Al2O3 ALD

during which the TMA and pump valves are closed, the pressure first continues at a decreasing rate, then flattens, then decreases at a nearly constant rate. We attribute the pressure rise to the deposition reaction, which is known to produce approximately 3/2 moles of CH_4 for every mole of TMA consumed [10], and we attribute the subsequent decrease in pressure to a leak across the pump valve. Thus we can divide the hold into two regimes: a reaction regime (pressure rising, flattening, and beginning to decrease) and a saturation regime (pressure decreasing at a nearly constant rate). The length of the reaction phase (time to saturation) increases from ~10 min in ALD cycle 1 (Fig. 8a) to ~13 min in cycle 16 (Fig. 8b) to ~18 min in cycle 40 (Fig. 8c), as expected for diffusion-reaction in a porous NP network with pores gradually shrinking over the course of the ALD process due to Al_2O_3 deposition.

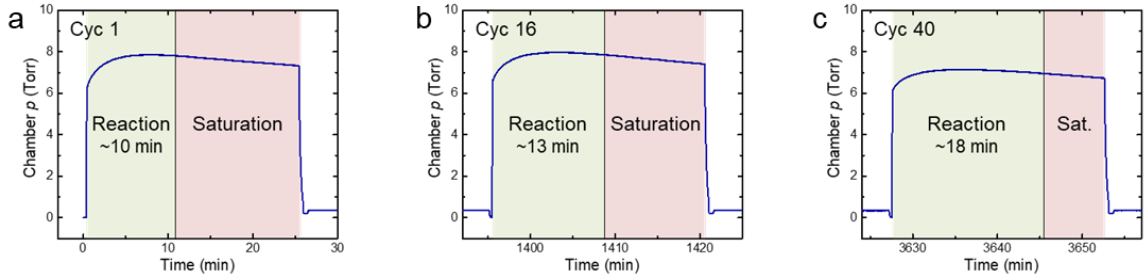

Fig. 8 — TMA dose pressure traces during Al_2O_3 ALD infilling of Al_2O_3 porous compacts: (a) cycle 1, (b) cycle 16, (c) cycle 40

3.4 ALD infilling of Al_2O_3 porous compacts with ZnO

Two Al_2O_3 compacts were simultaneously infilled with ALD using a DEZ partial pressure of ~7 Torr, an H_2O partial pressure of ~8 Torr, and hold and purge times of 25 and 21 min, respectively, for both precursors. The deposition temperature was ~150 °C, and the number of Al_2O_3 ALD cycles was 20, so that the total ALD process time was ~30 hr. Fig. 9 shows photographs of a compact before (Fig. 9a) and after (Fig. 9b) ZnO ALD. Unlike the Al_2O_3 infill process, the ZnO infill process resulted in a significant color change from off-white to dark brown-gray. The mass gains of the two compacts are 43% and 47% for an average of 45%, which if we assume a uniform infill of the porous compact, translates to a reduction in the porosity from ϕ = 49% to ϕ = 32% and a coating thickness of 5.7 nm, or an ALD growth per cycle (GPC) of 2.9 Å/cyc.

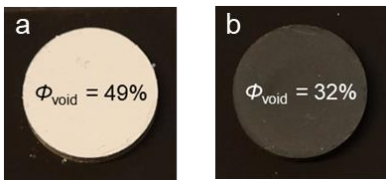

Fig. 9 — Photographs of Al2O3 porous compacts (a) before ALD and (b) after Al2O3 ALD

Fig. 10 shows ALD chamber pressure traces during DEZ doses. During ZnO ALD cycle 1 (Fig. 10a), the DEZ dose pressure trace is similar to the TMA dose pressure traces above. During the DEZ pulse (the first 50 s of the dose), the pressure rises sharply as DEZ fills the chamber. Subsequently, during the 25 min DEZ hold during which the DEZ and pump valves are closed, the pressure first continues at a decreasing rate, then flattens, then decreases at a nearly constant rate. As the ALD run progresses, however, the flattening and decreasing regimes gradually disappear. For example, in cycle 4 (Fig. 10b), there is no clear decreasing regime, and in cyc 20 (Fig. 10c), there is not even a clear flattening regime. These later-cycle pressure traces suggest that the DEZ diffusion-reaction process does not saturate.

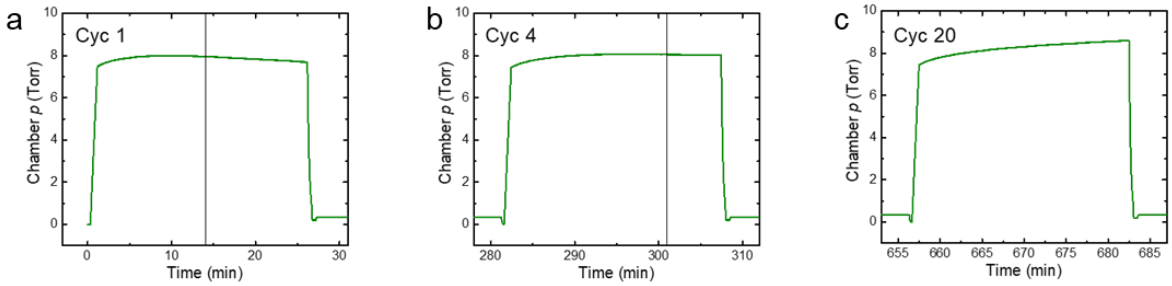

Fig. 10 — DEZ dose pressure traces during ZnO ALD infilling of Al_2O_3 porous compacts: (a) cycle 1, (b) cycle 4, (c) cycle 20

To understand the coating produced by the DEZ/H_2O ALD infill process, we characterized the nominally ZnO-infilled Al_2O_3 porous compact (Fig. 11a) via XRD (Fig. 11b) and SEM/EDS (Fig. 11c). For comparison, we produced an alternative Al_2O_3/ZnO nanocomposite by coating a powder of the Al_2O_3 NPs with ZnO at ~150 °C using a rotary particle atomic layer deposition (pALD) reactor—which agitates the powder so that it can be completely coated with a DEZ hold time of merely 2 min—and then pressing the resultant Al_2O_3/ZnO core/shell NP powder into a porous compact (Fig. 11d), and we characterized this nanocomposite by XRD (Fig. 11e) and SEM/EDS (Fig. 11f) as well. As expected, XRD pattern of the pALD-produced nanocomposite contains Al_2O_3 and ZnO peaks, and the cross-sectional SEM/EDS map shows uniform Zn Kα signal throughout the depth of the nanocomposite. In contrast, the XRD pattern of the ALD-infill-produced nanocomposite contains a Zn (100) peak in addition to Al_2O_3 and ZnO peaks, and the SEM/EDS map contains a Zn-poor band across the center of the cross-section. These results suggest that the deposition-reaction does not saturate because the DEZ decomposes, yielding Zn metal impurities in the coating and preventing complete infiltration.

4. CONCLUSION

Via rotary pALD, we were able to deposit Au NPs on both TiN and TiO_2 NP powders. We found that the quantity of Au deposited could be increased by three methods: moving the NP powder substrate closer to the pALD reactor inlet, increasing the Me_3AuPMe_3 dose, and, in the case of coating TiO_2, pre-coating the NP powder substrate with Al_2O_3 by pALD prior to Au pALD. The Au-coated TiO_2 NP powder exhibited LSPR absorption peaking near 550 nm, and a sample pre-coated with Al_2O_3 at 110 °C exhibited the strongest absorption. Future experiments should focus on improving the spatial uniformity and run-to-run consistency of Au depostion and should include an investigation into the thermal stability of Me_3AuPMe.

The results of our study of ALD infilling of macroscopic nanoporous solids suggest that uniform complete infilling is in fact possible provided that the ALD precursors are sufficiently stable under the required ALD conditions. In the case of infilling Al_2O_3 with Al_2O_3, TMA is highly stable at the deposition temperature (~150 °C), which allows it to infiltrate the entire porous compact over the course of the 25 minute hold

without decomposing, resulting in TMA dose pressure traces and porous compact mass gains consistent with uniform complete infilling. In contrast, DEZ lacks the stability required for a 25 minute hold at ~150 °C. Our ZnO rotary pALD experiment, however, revealed that when the hold time is reduced to 2 min, it is possible to conformally coat Al_2O_3 NP powder with a relatively pure and uniform ZnO coating at ~150 °C. In future ZnO ALD infilling experiments, the deposition temperature should be reduced in an effort to increase the DEZ lifetime to 25 minutes or longer.

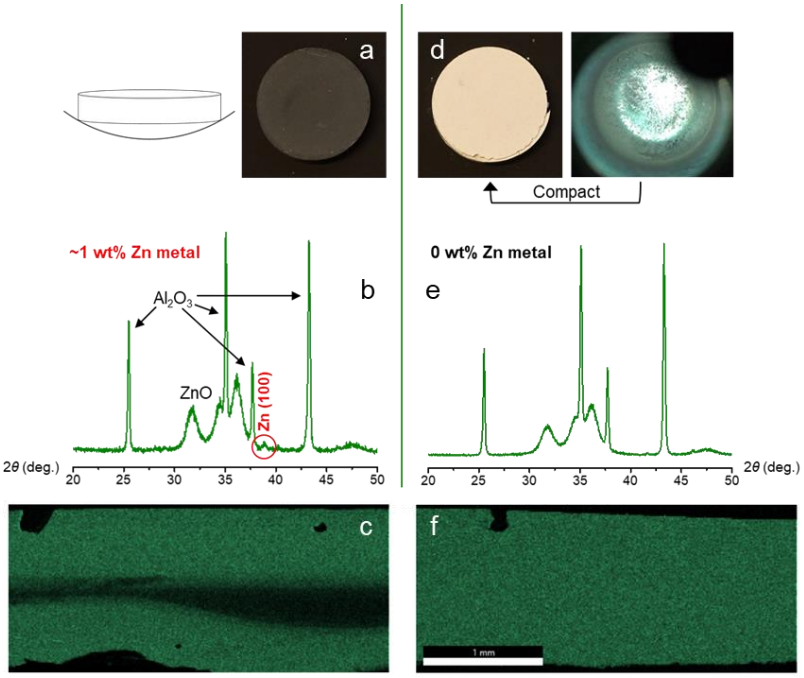

Fig. 11 — (a,b,c) Photograph, XRD, and SEM/EDS cross-sectional Zn Kα map, respectively, of ZnO-infilled Al2O3 porous compact. (d,e,f) Photograph, XRD, and SEM/EDS cross-sectional Zn Kα map, respectively, of compact formed by pressing Al2O3/ZnO core/shell NPs produced by pALD.

REFERENCES

1. Dabbousi, B. O.; Mikulec, F. V; Heine, J. R.; Mattoussi, H.; Ober, R.; Jensen, K. F.; Bawendi, M. G. "(CdSe)ZnS Core−Shell Quantum Dots: Synthesis and Characterization of a Size Series of Highly Luminescent Nanocrystallites". *J. Phys. Chem B* **1997**, *101*, 9463. DOI: 10.1021/jp971091y.

2. Hunter, K. I.; Held, J. T.; Mkhoyan, K. A.; Kortshagen, U. R. "Nonthermal Plasma Synthesis of Core/Shell Quantum Dots: Strained Ge/Si Nanocrystals". *ACS Appl. Mater. Interfaces* **2017**, *9*, 8263. DOI: 10.1021/acsami.6b16170.

3. Weimer, A. W. "Particle Atomic Layer Deposition". *J. Nanopart. Res.* **2019**, *21*, 9. DOI: 10.1007/s11051-018-4442-9.

4. Longrie, D.; Deduytsche, D.; Detavernier, C. "Reactor Concepts for Atomic Layer Deposition on Agitated Particles: A Review". *J. Vac. Sci. Technol. A* **2014**, *32*, 010802. DOI: 10.1116/1.4851676.

5. Baturina, O. A.; Feygelson, B.; Greenberg, B.; Wheller, V.; Boltersdorf, J.; McCool, G.; Giles, S.; Fulton, A.; Lundin, J.; Webb, A.; Govorov, A. "Visible-Light Activated Sensor for Detection of Chemical Warfare Agent Simulants". Memorandum Report: final report for CB10778 program funded by DTRA. **2023**.

6. Griffiths, M. B. E.; Pallister, P. J.; Mandia, D. J.; Barry, S. T. "Atomic Layer Deposition of Gold Metal". *Chem. Mater.* **2016**, *28*, 44. DOI: 10.1021/acs.chemmater.5b04562.

7. Cendejas, A.; Moher, D.; Thimsen, E. "Modeling atomic layer deposition process parameters to achieve dense nanocrystal-based nanocomposites". *J. Vac. Sci. Technol. A* **2021**, *39*, 012406. DOI: 10.1116/6.0000588.

8. Yanguas-Gil, A.; Elam, J. W. "Self-Limited Reaction-Diffusion in Nanostructured Substrates: Surface Coverage Dynamics and Analytic Approximations to ALD Saturation Times". *Chem. Vap. Depos.* **2012**, *18*, 46. DOI: 10.1002/cvde.201106938.

9. Manandhar, K.; Wollmershauser, J. A.; Boercker, J. E.; Feigelson, B. N. "Growth per cycle of alumina atomic layer deposition on nano- and micro-powders". *J. Vac. Sci. Technol. A* **2016**, *34*, 021519. DOI: 10.1116/1.4941918.

10. Puurunen, R. "Surface chemistry of atomic layer deposition: A case study for the trimethylaluminum/water process". *J. Appl. Phys.* **2005**, *97*, 121301. DOI: 10.1063/1.1940727.